NUCLEAR STRUCTURE -- EXPERIMENTAL

Inelastic Scattering of 210 MeV ^{6}Li Ions to the First Excited 2^{+} States of ^{12}C, ^{28}Si, and ^{58}Ni

A. Nadasen,[a] J.S. Winfield, R.M. Ronningen, M. McMaster,[a] M. Fingal,[a] J. Tavormina,[a] P. Schwandt,[b] F.D. Becchetti[c], J.W. Janecke,[c] and R. E. Warner[d]

It has long been advocated[1] that heavy-ion optical model potentials (OMPs) determined from elastic scattering should be tested for their ability to reproduce cross sections for other reaction channels, since the form factors may probe different regions of the nuclear potential. For this reason, we have measured the inelastic scattering of 210-MeV ^{6}Li ions from ^{12}C, ^{28}Si and ^{58}Ni over wide angular ranges in order to evaluate the unique potentials obtained in Ref. 2. If the unique OMPs have the correct strength and gradient in the region of the strong absorption radius, they should generate form factors that reproduce the inelastic scattering data. The measurements were made using the beams from the K500 cyclotron and the scattered particles were detected with the S320 magnetic spectrometer and its standard focal plane detection system. The energy resolution was typically 400 to 500 keV, sufficient to resolve the 2^{+} excited state from adjacent levels for each target.

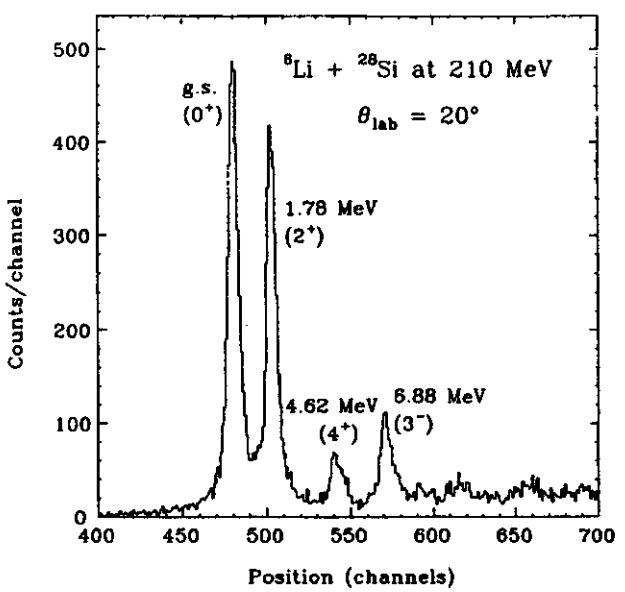

FIG. 1: Energy spectrum for the scattering of 210-MeV ^{6}Li ions from ^{28}Si at $\theta_{lab} = 20°$.

Figure 1 shows the spectrum obtained for ^{28}Si at $\theta_{lab} = 20°$. The yields of 4^{+}(4.62 MeV) and 3^{-}(6.88 MeV) states are an order of magnitude weaker than those to the ground state and 2^{+}(1.78 MeV) channels. The angular distribution for the 4.44-MeV state of ^{12}C is represented by solid points in Fig. 2. The data extend from 6.8° to 60.6° (c.m.). Uncertainties are indicated with bars where they exceed the size of the points. The open circles represent the elastic scattering cross sections which were measured concurrently.[2] It is observed that the shape of the inelastic angular distribution is very similar to that of elastic scattering, having smooth exponential fall-off at large angles, which characterizes refractive elastic scattering. The angular distributions for the elastic and inelastic scattering from ^{28}Si and ^{58}Ni have features very similar to those of ^{12}C, except that the diffractive oscillations occur over larger angular ranges.

Both distorted-wave Born approximation (DWBA) and coupled channels analyses were carried out for the data, based on the collective model description of the 2^{+} states. Such analyses provide information on the deformation of the nuclei, and usually the deformation parameters, β_2, are extracted. However, when comparing excitations induced by different projectiles, it is more appropriate to compare deformation lengths, $\beta_2 R$, rather than deformation parameters, β_2. Therefore the constraint $\beta_R R_R = \beta_I R_I = \beta_C R_C = \beta_2 R_R$ was imposed on all calculations.

The DWBA analysis was carried out using the code DWUCK4.[3] We used the standard derivative collective-model form factor to describe the interaction. The coupling term had the form:

$$F_N(r) = \frac{d}{dr}[\beta_R R_R V(r) + i\beta_I R_I W(r)]$$

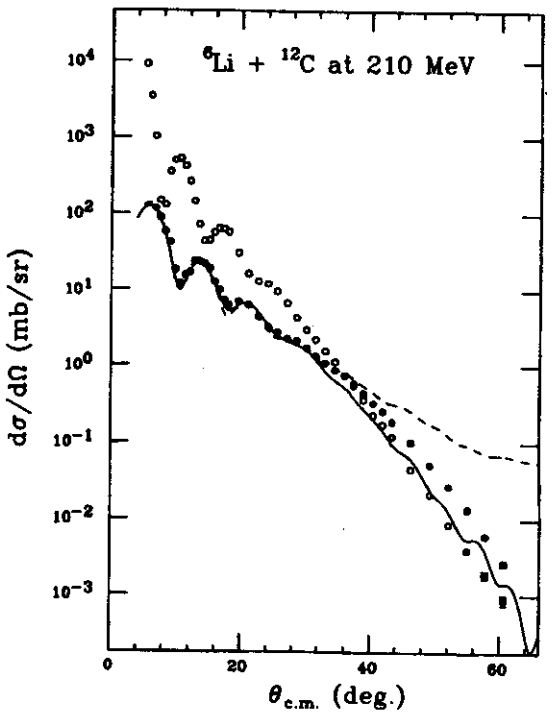

FIG. 2: Cross section angular distributions for inelastic scattering of 210-MeV ^{6}Li ions to the first excited 4.44-MeV state of ^{12}C (solid dots) and elastic scattering (open circles). Also shown are DWBA predictions of the inelastic scattering cross sections using the unique optical model potentials (solid line) and the ambiguous potentials (dashed line). The calculations are normalized to the data by the β_2 values derived in the analysis.

where β_R and β_I are the real and imaginary quadrupole deformation parameters. $V(r)$ and $W(r)$ are the real and imaginary optical model potentials derived from elastic scattering data. R_R and R_I are the radii of the potentials defined by $R_I = r_o A^{\frac{1}{3}}$ and $R_I = r_w A^{\frac{1}{3}}$. As is customary, a Coulomb potential energy term was also included.

The distorted waves for the incoming and outgoing ^{6}Li particles were generated with OMPs derived from the elastic scattering data measured concurrently[2] (see Table I). Various combinations of the unique potentials and the different ambiguous sets were tried in the calculations.

The results of the calculations are shown in Fig. 2. The solid line represents calculations with the unique potentials in both the entrance and exit channels. These potentials are listed in Table I. Use of any of the ambiguous potentials in either channel causes the calculation to deviate significantly from the data for large angles. An example of such a calculation is shown by the dashed line in Fig. 2. By comparing data with calculations, magnitudes of $\beta_2 R$ were extracted. These values are listed in Table II.

TABLE I: Unique optical model potentials[2] used in the DWBA calculations for the first excited (2^+) level. The convention $R_x = r_x A^{\frac{1}{3}}$ is used.

Target	V (MeV)	r_o (fm)	a_o (fm)	W_v (MeV)	r_w (fm)	a_w (fm)
^{12}C	113.5	1.305	0.793	34.2	1.682	0.784
^{28}Si	125.2	1.299	0.836	31.4	1.703	0.822
^{58}Ni	174.5	1.136	0.907	32.0	1.607	0.806

TABLE II: Comparison of $\beta_2 R$ and q_{20} values obtained from the present analyses with adopted values.[5]

Target	$\beta_2 R$ from DWBA analysis (fm)	$\beta_2 R$ from coup. ch.analysis (fm)	$\beta_2 R$ from adopted β_2(Ref. 5) (fm)	q_{20} from present work (eb)	q_{20} from adopted B(E2) (Ref. 5) (eb)
^{12}C	1.03	-1.13	1.63	-0.067±0.003	0.064
^{28}Si	1.21	-1.15	1.48	-0.19±0.01	0.181
^{58}Ni	0.76	+0.80	0.85	+0.34±0.01	0.346

The coupled-channels calculations were carried out using the code ECIS79.[4] In these calculations, ^{58}Ni was assumed to be a vibrational nucleus and the first-order vibrational model was used to couple the ground state to the 2^+ state. ^{12}C and ^{28}Si were treated as rigid rotors, and couplings involving both the excitation and de-excitation between the ground state and 2^+ level, including terms of order $(\beta_2)^2$, were used. The starting optical model parameters were those given in Table I and the starting β_2-values were obtained from the literature.[5] Searches were carried out on the optical model parameters as well as the β_2 values, in order to minimize x^2 for both the elastic and inelastic scattering data.

Figure 3 shows the calculations together with the data for ^{58}Ni. The calculations for the ground state (dashed lines) compare very well with the optical model analyses of Ref. 2, both in terms of visual observation and the objective x^2 criterion. The fits for ^{28}Si and ^{12}C are similar. In all cases, the coupled-channels analyses did not significantly change the unique OMPs, an indication of the validity of these potentials. The derived $\beta_2 R$ values are also given in Table II.

The $\beta_2 R$ values derived from the two types of analyses are consistent with each other. While there is reasonable agreement between the present results and electromagnetic measurements[5] for ^{58}Ni, the $\beta_2 R$ values we obtain for ^{12}C and ^{28}Si are much lower. In view of the large scatter of the results of different investigations, it is not clear that one can assign much significance to the $\beta_2 R$ values extracted from experiments with hadronic probes.

We have calculated the transition quadrupole moments using the formula

$$q_{20} = \frac{Ze\int r^2 V(r,\theta) Y_{20}(\theta) d\vec{r}}{\int V(r,\theta) d\vec{r}}$$

with the parameters obtained from the coupled-channels analyses. These are also listed in Table II. They are in excellent agreement with those deduced from the B(E2) values of Raman *et al.*[5] (last column in Table II).

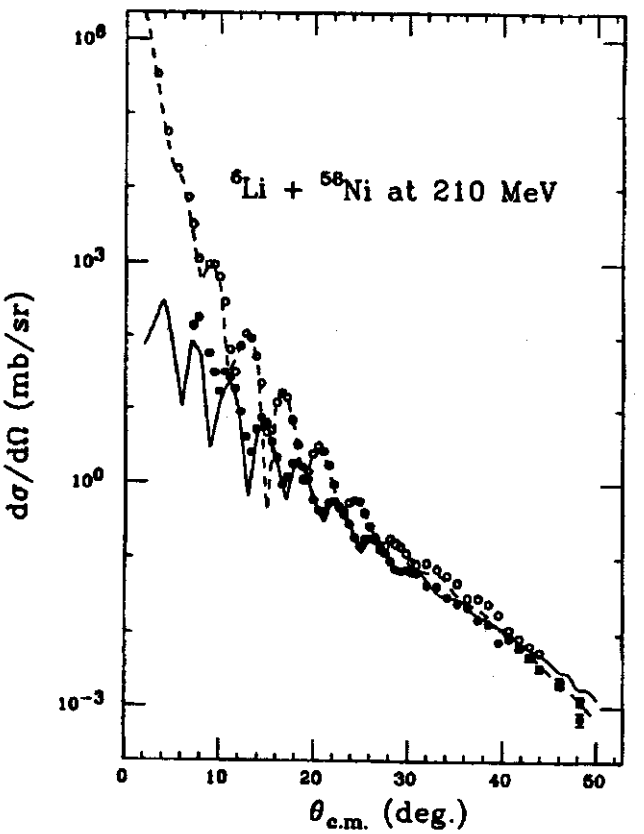

FIG. 3: Cross section angular distributions for the elastic (open circles) and inelastic (solid dots) scattering of 210-MeV ^{6}Li ions from ^{58}Ni. Coupled-channels calculations for the elastic (dashed line) and inelastic (solid line) data are also shown.

This could be an indication that it may be more appropriate to compare this more fundamental quantity, rather than the deformation length, with other measurements.

References

a. University of Michigan, Dearborn, Michigan 48128

b. Indiana University Cyclotron Facility, Bloomington, Indiana 47405

c. University of Michigan, Ann Arbor, Michigan 48109

d. Oberlin College, Oberlin, Ohio 44074

1. G.R. Satchler, *Proceedings from the International Conference on Reactions between Complex Nuclei, Nashville* (Amsterdam, 1974) p. 171.

2. A. Nadasen *et al.*, Phys. Rev. C37, 132 (1988); *ibid.* C39, 536 (1989).

3. P.D. Kunz, DWUCK4 (unpublished); extended version of J.R. Comfort (unpublished).

4. J. Raynal, computer code ECIS79, SEN-Saclay, 1979 (unpublished).

5. S. Raman, *et al.*, At. Data Nucl. Data Tables 36, 1 (1987).

Heavy-Ion Transfer Reactions and Optical Model Ambiguities

J.S. Winfield, S.M. Austin, G.M. Crawley, A. Nadasen,[a] C.A. Ogilvie, and G.R. Satchler[b]

Phenomenological optical model potentials are important both in their own right (for example, from them the strong absorption radius and total reaction cross section may be deduced), and as necessary ingredients in spectroscopic studies of inelastic excitations and transfer reactions. In addition, the phenomenological approach complements and can guide a first-principles (folding model) calculation of the nuclear mean field.

In the past, optical model analyses of heavy-ion elastic scattering data have been plagued by ambiguities in the parameters, principally because the data are sensitive only to the tail of the effective nuclear potential. However, as the bombarding energy is increased, elastic scattering begins to probe the potential at smaller and smaller radii as nuclei become more transparent and the contribution from farside scattering increases.[1] From studies[2] of α-scattering, it is known that optical model parameters are greatly constrained by measurements into the farside-scattering region. Recently, this has also been shown for 210 MeV ^{6}Li elastic scattering,[3] for which unique Woods-Saxon potentials have been found for targets ranging from ^{12}C to ^{90}Zr. Elastic scattering data for heavier ions are still not sufficient to remove all ambiguities, and several families of potentials give equally good fits. A new approach is to use transfer reaction data to help constrain potentials found from elastic scattering. The underlying idea is that the two reactions are sensitive to different radial regions of the potential. One compares data with the shapes and magnitudes of the transfer cross sections predicted by DWBA calculations after optical potentials have been determined from elastic scattering data. Some work along these lines has been done by Horen and Fernandes *et al.*[4] for ^{18}O+^{28}Si-induced transfer reactions at E/A = 20 MeV. They showed that a surface-transparent potential which fits the somewhat limited elastic scattering data was unrealistic, since it grossly overpredicts the transfer cross sections.

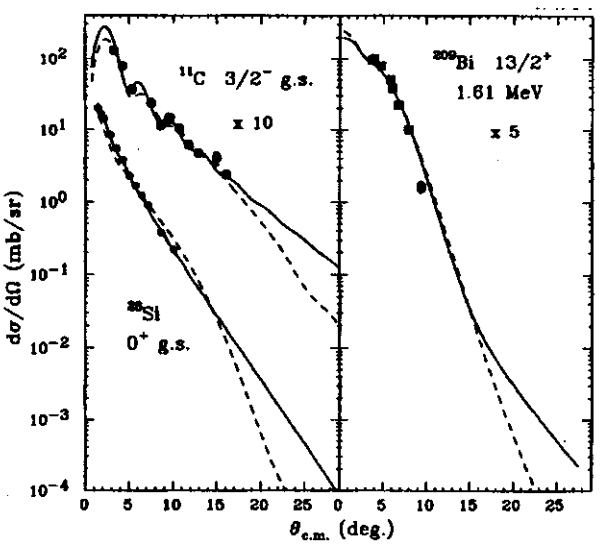

FIG. 1: Differential cross section angular distributions for the reactions ^{12}C(^{12}C,^{13}C)^{11}C, ^{27}Al(^{12}C,^{11}B)^{28}Si and ^{208}Pb(^{12}C,^{11}B)^{209}Bi at E/A = 50 MeV. The curves are DWBA predictions with optical model potentials taken from the literature (see Ref. 5 for details). They have been normalized separately to the data.

We originally became interested in this problem while testing the validity of DWBA for various single-nucleon transfer reactions induced by E/A = 50 MeV ^{12}C.[5] For the reactions on the ^{12}C and ^{27}Al targets studied, optical model potentials with deep imaginary wells underpredicted the data by factors of 2 to 3, while shallow imaginary potentials taken from the literature gave reasonable agreement. Furthermore, it appeared that large-angle data could discriminate between the potentials based on the shape of the angular distribution (see Fig. 1). However, the potentials concerned would also predict quite different elastic scattering cross sections at E/A = 50 MeV, and if data were available at this energy they presumably would be sufficient to select one potential or the other.

More refined investigations have concentrated on the ^{12}C(^{12}C,^{13}C)^{11}C reaction. Rather than taking potentials derived from different elastic scattering data sets, a particular data set (e.g. one for E/A = 30 MeV from Ref. 6) is chosen for re-analysis, and we find both shallow (W ~ 25 MeV) and deep (W > 50 MeV) imaginary well

solutions to the data. Typically, the fits to the elastic data have similar x^2, although the angular distributions are not identical. These potentials are then used in DWBA transfer calculations, and the results compared to experiment.

An example at E/A = 50 MeV is shown in Fig. 2. The differences between the transfer predictions from the two potential types are smaller than our original study suggested, being at the 30 to 40% level for E/A = 50 MeV. However, the sensitivity to optical model parameters increases with bombarding energy. Calculations at E/A = 85 MeV (not shown) indicate that even a few transfer cross section measurements beyond $\theta_{c.m.} > 5°$ should make possible an unambiguous determination of $^{12}C + ^{12}C$ optical model potentials.

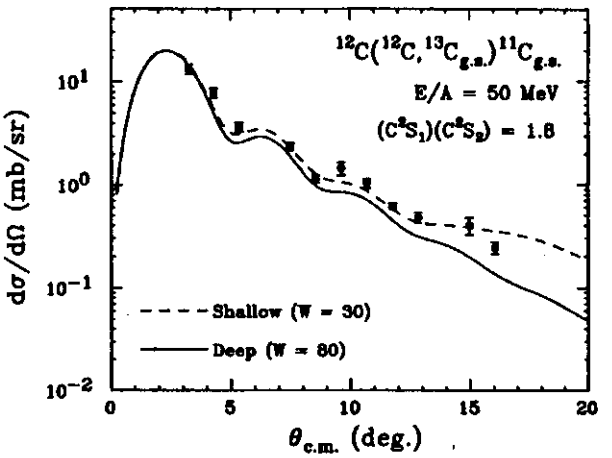

FIG. 2: Differential cross section angular distributions for $^{12}C(^{12}C,^{13}C)^{11}C$ at E/A = 50 MeV. The curves are DWBA predictions with optical model potentials taken from fits to elastic scattering data[6] at E/A = 30 MeV. The depths of the imaginary wells, W, are indicated in MeV. The product of target and projectile spectroscopic factors has been taken as 1.8 for both calculations.

References

a. On leave from University of Michigan, Dearborn.

b. Oak Ridge National Laboratory.

1. P. Roussel-Chomaz *et al.*, Nucl. Phys. A477, 345 (1988); J. Barrette, J. Phys. C4 47, 141 (1986).

2. D.A. Goldberg and S.M. Smith, Phys. Rev. Lett. 29, 500 (1972); D.A. Goldberg *et al.*, Phys. Rev. C 10, 1362 (1974).

3. A. Nadasen *et al.*, Phys. Rev. C 37, 132 (1988); 39, 536 (1989).

4. D.J. Horen *et al.*, Z. Phys. A 328, 189 (1987); M.A.G. Fernandes *et al.*, Phys. Rev. C 33, 1971 (1986).

5. J.S. Winfield *et al.*, Phys. Rev. C 39, 1395 (1989).

6. M. Buenerd *et al.*, Nucl. Phys. A424, 313 (1984).

Measurement of the Γ_γ / Γ_p Branching Ratio for the 7.8 MeV, T=3/2, J=5/2$^+$ State in ^{23}Mg

R. Harkewicz, J. Gorres[a], D. Mikolas, D.J. Morrissey, J.A. Nolen, B. Sherrill, and M. Wiescher[a]

The reaction, ^{22}Na$(p,\gamma)^{23}$Mg (Q = 7.58 MeV), is of considerable interest for understanding the hot NeNa-cycle and the rp-process in explosive stellar environments.[1] Of particular importance are the reaction rates for determining the abundances of ^{22}Na in such burning events, because the decay of ^{22}Na ($t_{1/2}$=2.6 y), after the freeze-out provides an attractive mechanism for the formation of ^{22}Ne-enriched Neon isotopic anomalies (NeE) observed in meteoritic inclusions.[2] The first excited state of ^{23}Al was measured with the (^{7}Li, ^{8}He) reaction on ^{24}Mg using the S320 spectrograph.[3]

The next step, detailed in this paper, is to obtain the ratio of the γ-decay width to the proton width, Γ_γ / Γ_p, for the 7.8 MeV, T = 3/2, J^π = 5/2$^+$ state in ^{23}Mg by measuring the β-delayed proton spectrum of ^{23}Al. This state of ^{23}Mg is the IAS of the ^{23}Al ground state. One would expect the main branch of ^{23}Al β^+-decay to proceed to this ^{23}Mg Isobaric analog state (IAS), which is proton-unbound by 219 keV. The proton decay of this level is isospin-forbidden; hence, the proton branch should be small. Gough deduced an upper limit; $\Gamma_\gamma / \Gamma_p > 50$.[4] In general, the β-delayed proton decay of ^{23}Al selects states with a large proton width and spins of 3/2$^+$, 5/2$^+$ and 7/2$^+$ corresponding to s- and d-wave resonances in the ^{22}Na(p,γ) reaction. Therefore, measurement of the β-delayed proton branches would provide valuable information to guide the studies of the reaction rate of ^{22}Na(p,γ) ^{23}Mg. In particular, if isospin mixing increases Γ_p for the IAS, it could be important for the process. The low energy of this possible resonance (Q = 210 keV) makes information on its width extremely important.

^{23}Al nuclei were produced by fragmenting ^{36}Ar at E/A = 35 MeV (from the K500 cyclotron) with a 51 mg/cm^2 natural magnesium target. The ^{23}Al nuclei were separated by the RPMS and focused on a silicon detector telescope at the focal plane of the spectrometer. The silicon telescope consisted of the sequence of a 100 μm, 100 μm, 50 μm, 20 μm, 30 μm, 75 μm, 500 μm and 1000 μm detectors operated in vacuum at -20°C.

The ions entering the telescope were identified by a combination of energy-loss in the first two silicon detectors, and by time-of-flight through the RPMS. When an ^{23}Al was identified by the front-end computer, the cyclotron beam was shut off within 50 μs for three half-lives (approximately 1.5 seconds) by changing the RF phase in one of the cyclotron dees. The gain of the silicon detector preamps was simultaneously increased by a factor of 10 in order to observe the decay products. Counting the number of decay protons per incoming ^{23}Al gives a direct measurement of the branching ratio. Thin silicon detectors were used in the central part of the silicon telescope to reduce the contribution of pile-up of the positron on the proton signal.

The β-decay branch of the ground state of ^{23}Al to the IAS in ^{23}Mg is predicted to be 20%,[5] and Gough's upper limit for the proton gamma branching is 50. Hence, we would expect 1 in 250 ^{23}Al's to decay via proton decay. Therefore *a minimum of 2500 nuclei would have to be observed* to produce a 10-count proton peak, assuming a 100% detection efficiency. Unfortunately, after approximately 24 hours of beam time, little more than 400 ^{23}Al's were observed, thus prohibiting a proton gamma branching determination.

We believe we can increase the ^{23}Al count rate by upgrading the RPMS and also using different beams. Refurbishment of the RPMS is presently underway,[6] along with mapping of the magnetic components of the device to facilitate its tuning. This would improve its overall performance, including transmittance of reaction products through the separator. Acceleration of sulfur or silicon beams by the NSCL cyclotrons would also provide higher yields of ^{23}Al.

References

a. University of Notre Dame, South Bend, Indiana.

1. R.K. Wallace and S.E. Woosley, Astrophys. J. Supp. Ser. 45, 389 (1981).

2. P. Eberhardt *et al.*, Astrophys. J. Lett. L169, 234 (1979).

3. M. Wiescher *et al.*, Nucl. Phys. A484, 90 (1988).

4. R.A. Gough *et al.*, Phys. Rev. Lett. 28, 510 (1972).

5. B.A. Brown, private communication.

6. R. Harkewicz, "Recent Developments with RPMS," *NSCL Annual Report* (1988).

Energy Levels of Light Nuclei

L. Heilbronn, A. Galonsky, X. Yang, F. Deák,[a] A. Kiss,[a] and Z. Seres[b]

Introduction

A number of experimental techniques have been developed to measure the energies and widths of states of various nuclei. Some of these methods are applicable only to particle-unbound states, while others can be generally applied to both particle-bound and particle-unbound states. All these methods share a common trait in that they produce a two-body final state, which allows the energy and width of a particular state to be determined by measuring the spectrum of just one reaction product. These methods are not very applicable to nuclei produced in heavy-ion collisions since they generally result in a *many*-body final state. An alternate method which *is* applicable is the method of sequential decay spectroscopy, in which the two-body decay of an unbound state is detected by observing both decay products.

We have measured the energies and widths of two states that decay by neutron emission using the method of sequential neutron decay spectroscopy. This method separates one excited state from all other states produced in the collision by using a coincidence technique that gives us the momenta of the neutron and of the daughter nucleus. The vector difference of those momenta determines the decay energy and therefore the excitation energy of that state. This result is independent of the laboratory kinetic energy of the parent nucleus.

When the decay energy is small compared to the kinetic energy of the parent, a large fraction of the decay neutrons is kinematically focused along the direction of the daughter fragment.[1] By placing our fragment detector and neutron detector in a colinear alignment, we are then able to take advantage of the kinematical focusing, hence increasing our coincidence rate without diminishing our resolution.

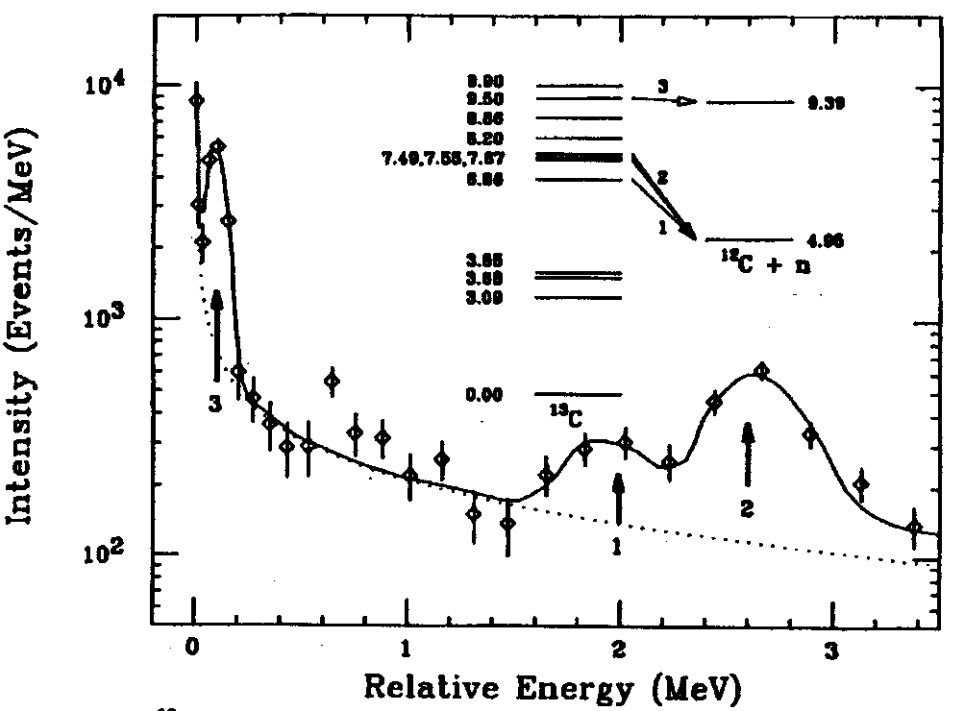

FIG. 1: Relative energy spectrum for ^{12}C + neutron at 15°. The solid line indicates the fit to the data and the dotted line indicates the background. The labeled peaks correspond to decays from ^{13}C that are illustrated in the level diagram.

When using the colinear alignment, the neutron and fragment momentum vectors are parallel. This enables us to determine the decay energy by measuring the relative energy between the daughter fragment and the neutron.

Experimental Technique

We observed neutrons and fragments in coincidence at 15° and at 31° produced by collisions of ^{14}N projectiles at 35 MeV/nucleon with an Ag target. Fragment species and energy were determined by using silicon telescopes. Neutron energies were determined by a time-of-flight technique that used the neutron signal and fragment signal as the start and stop of a timing circuit.

Figure 1 contains a relative energy spectrum for ^{12}C fragments and neutrons at 15°. The peak at $E_{rel} \approx 100$ keV comes from the decay of the 9.50-MeV ($\Gamma = 5$ keV) state in ^{13}C to the first excited state in ^{12}C. The peak at $E_{rel} \approx 2$ MeV is due to the decay of the 6.86-MeV ($\Gamma = 6$ keV) state, and the peak at $E_{rel}\Gamma \approx 2.3$ MeV is from the decay of a group of three states at 7.49 MeV ($\Gamma < 5$ keV), 7.55 MeV ($\Gamma = 1.2$ keV), and 7.69 MeV ($\Gamma = 70$ keV) in ^{13}C. The solid line shows a fit to the data using the above parameters and the geometry of the detectors, and the dotted line shows the background used in the fit. For each peak in Fig. 1 the level width is much smaller than the instrumental resolution at the corresponding peak energy. Hence, the good fit to these peaks establishes the accuracy of the computation.

Results

Figure 2 shows a relative energy spectrum for ^{7}Be fragments and neutrons at 15°. The dot-dashed and dotted lines show the two backgrounds used for the fitting. The dashed line shows the fit to the data using the dot-dashed background, while the solid line indicates the fit using the dotted background.

The peak at 0.28 MeV is from the decay of the 19.24-MeV state in ^{8}Be. Most of the counts in the region between 0 and 0.5 MeV are from the decay of the 19.24-MeV state. The fact that a large number of counts from this decay are below 200 keV is an interesting consequence of the relatively large width of the state and the kinematical focusing of neutrons into our detectors.

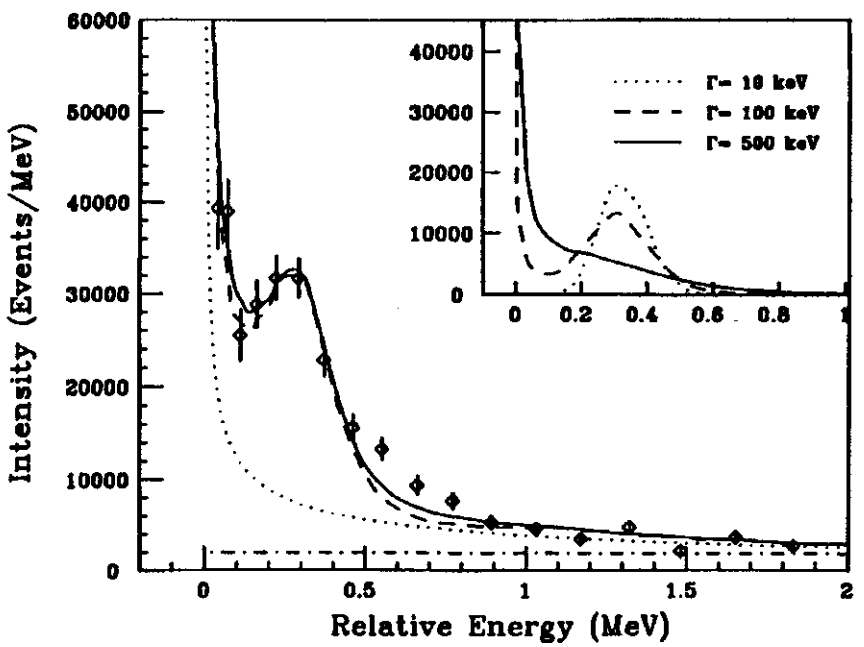

FIG. 2: Relative energy spectrum for ^{7}Be + neutron at 15°. The dashed line shows the fit using the dot-dashed background, while the solid line shows the fit to the data using the dotted background (see text). The peak at 0.28 MeV comes from the decay of the 19.24-MeV state ($\Gamma \approx 200$ keV) in ^{8}Be. Inserted in the upper right hand corner is a simulation of the decay of the 19.24-MeV state for three assumed widths. There is no background included in the simulations.

The reported decay energy of the 19.24-MeV state to the ground state of ^{7}Be is 0.342 MeV and the reported width of the state is 230 keV.[2] Because the width is comparable to the decay energy, it is possible to have a decay with an energy significantly lower than 342 keV, although the probability of getting lower, off-resonance energies decreases with energy. However, as the decay energy decreases, the geometrical efficiency increases rapidly.[1] It is these two effects together which conspire to give the spectrum its shape between 0 and 0.2 MeV. These effects are also responsible for the fact that the peak value lies below the value for the relative energy of this decay. Included in the upper right corner of Fig. 2 are Monte Carlo simulations of the decay of this state for hypothetical widths of 10, 100, and 500 keV.

Due to the complicated nature of heavy-ion collisions, the exact physical nature of the background in relative energy spectra such as the one in Fig. 2 is unknown. However, a background generated from coincidences of neutrons and fragments emitted from thermal, moving sources has been used in similar analyses of relative *velocity* spectra (see Ref. 3, Fig. 2). The shape of this background is a Gaussian in velocity space. The result of transforming such a Gaussian background to energy space is shown by the dotted-line background in Figs. 1 and 2. In order to estimate the effect the background has on the determination of the level energy and width, the results obtained when using this background were compared to the results obtained from another type of background. The other background used is essentially a flat background; it is shown as the dot-dashed line in Fig. 2. Although these two backgrounds are similar in the high-energy tails of our spectra, they differ a great deal in the low-energy end, which is the region where our fitting is most sensitive. For both of the levels reported here, the energy and width determined with one background are well within uncertainties of the values obtained with the other background.

Figure 3 shows our best fit to the ^{8}Li + n data at 15° using the Gaussian background in velocity space. The peak at 0.2 MeV is from the decay of the 4.31-MeV state in ^{9}Li. Shown in the upper right hand corner of Fig. 3 is a plot of the region of interest. Both fits using each type of background are shown, using the same convention used in Fig. 2.

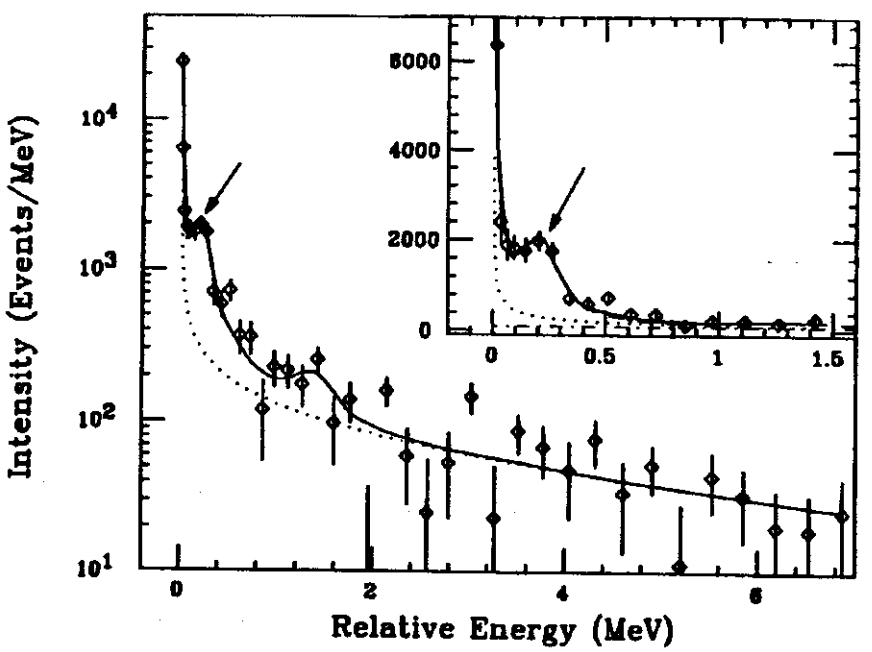

FIG. 3: Relative energy spectrum for ^{8}Li + neutron at 15°. The solid line shows the fit to the data, and the dotted line shows the background used in the fitting. The peak at 200 keV (indicated by the arrow) is from the decay of the 4.31-MeV state in ^{9}Li to the ground state of ^{8}Li.

As one can see, the fits are almost identical, although the extracted parameters from the two fits differ by small amounts. As was the case with the 19.24-MeV state in ^{8}Be, these parameters were well within uncertainties of each other, however.

TABLE I: Energies and widths determined from the best fits to our data for the 19.24-MeV state of ^{8}Be and the 4.31-MeV state in ^{9}Li.

Level Energies and Widths

Isotope	Level Energy (MeV)	Decay Energy (keV)	Width (keV)
^{8}Be	19.234±.012 [a]	336	210±35 [a]
	19.21 [b]	312	208±30 [b]
	19.260±.030 [c]	362	220±30 [c]
	19.220±.030 [d]	322	265±30 [d]
^{9}Li	4.296±.015 [a]	233	60±45 [a]
	4.310±.030 [e]	247	250±30 [e]
	4.310±.020 [f]	247	100±30 [f]

a – this work
b – Ref. 6
c – Ref. 7
d – Ref. 8
e – Ref. 9
f – Ref. 10

Table I contains the energies and widths determined from the best fits to our data for the 19.24-MeV state of ^{8}Be and the 4.31-MeV state in ^{9}Li. Once the best values were found for the energy and width for a particular isotope, angle, and background combination, the errors in those values were determined by the following method. A contour plot of the x^2 values vs. E and Γ was made. The extremes in E and Γ for the contour where x^2 increased by 1 defined the errors in the best values. This method allows us to include any correlated errors between E and Γ in the uncertainty we determine for each parameter. For the 19.24-MeV state in ^{8}Be, the values and errors reported in Table I are the weighted values and errors from the two angles where we had data (15° and 31°).

Comparisons with Other Results

Previously, the energy and width of the 19.24-MeV state in ^{8}Be were measured with the ^{7}Li(p,n)^{7}Be reaction,[5] the ^{9}Be(p,d)^{8}Be reaction,[6] the ^{9}Be(d,t)^{8}Be reaction,[7] and the ^{9}Be(^{3}He,α)^{8}Be reaction.[8] In all of these measurements, the energy and width were determined from an excitation function of the light particle emitted from a two-body final state. Both the energy and width we determined are within the errors of these previous measurements.

As shown in Table I, the energy of the 4.31-MeV state in ^{9}Li seems to be well established from two other reactions, the ^{7}Li(t,p)^{9}Li reaction[9,10] and the ^{11}B(^{6}Li,^{8}B)^{9}Li reaction,[11] both of which have a two-body final state.

Conclusions

By using the method of sequential neutron decay spectroscopy, which utilizes a colinear fragment-neutron detector alignment, we are able to detect both decay products of a fully accelerated, neutron-unbound fragment. The energies and widths we determined for the 19.24-MeV state in ^{8}Be and the 4.31-MeV state in ^{9}Li indicate that this method may be useful for measuring these parameters in other states where the decay energy is small.

References

a. Eötvös Lourand University, Budapest, Hungary

b. Central Research Laboratory for Physics, Budapest, Hungary

1. F. Deák *et al.,* Nucl. Instrum. Methods A258, 67 (1987).

2. F. Ajzenberg-Selove, Nucl. Phys. A490, 1 (1988).

3. A. Kiss *et al.,* Phys. Lett. 184B, 149 (1987).

4. P.R. Bevington, *Data Reduction and Error Analysis for the Physical Sciences,* (McGraw-Hill), p. 242.

5. H.W. Newson *et al.,* Phys. Rev. 108, 1294 (1957).

6. L.A. Kull, Phys. Rev. 163, 1066 (1967).

7. M.A. Oothoudt and G.T. Garvey, Nucl. Phys. A284, 41 (1977).

8. F. Ajzenberg-Selove *et al.,* Phys. Rev. C13, 46 (1976).

9. P.G. Young and R.H. Stokes, Phys. Rev. C4, 1597 (1971).

10. F. Ajzenberg-Selove, E.R. Flynn and O. Hansen, Phys. Rev. C 17, 1283 (1978).

11. R.B. Weisenmiller *et al.,* Nucl. Phys. A280, 217 (1977).

Doubly-Decoupled Bands in Odd-Odd Nuclei: Experiments and IBFFA Calculations

Wm.C. McHarris, W.-T. Chou and W.A. Olivier

Doubly-decoupled bands, i.e., odd-odd bands formed by coupling a decoupled $K=1/2$ proton state with a decoupled $K=1/2$ neutron state, were first characterized in ^{186}Ir by Kreiner *et al.*[1] Since then, many such bands have been characterized,[2] mostly in the Ta-Re-Ir region. Such bands are important to study, for there is an outside chance they may provide insight into the residual *p-n* interaction in moderately-heavy nuclei -- there should be less interference from the core than in other odd-odd systems. In the Ta-Re-Ir region these bands consist of the highly-distorted $\pi h_{9/2}[541\downarrow]$ state coupled to the less-distorted $\nu p_{3/2}[521\uparrow]$ state.

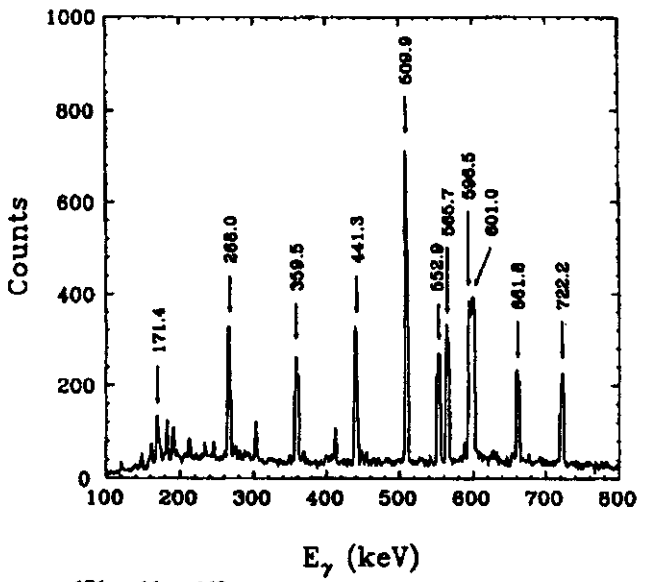

FIG. 1: ^{176}Re(^{16}O + ^{165}Ho) doubly-gated coincidence spectrum on the 171.4-keV group.

We used the ^{159}Tb(^{22}Ne,5*n* γ)^{176}Re, ^{159}Tb(^{20}Ne,5*n* γ)^{174}Re, and ^{139}La(^{40}Ar,5*n* γ)^{114}Re reactions with beams from the K500 cyclotron at MSU NSCL, and the ^{165}Ho(^{16}O,5*n* γ)^{176}Re and ^{165}Ho(^{16}O,7*n* γ)^{174}Re reactions from the tandem-linear accelerators at SUNY Stony Brook to study these nuclei via in-beam γ-ray spectroscopy. Compton-suppressed Ge detectors plus multiplicity filters were used to obtain a variety of coincidence spectra. An example of a gated coincidence spectrum, identifying transitions in the doubly-decoupled band in ^{176}Re, is shown in Fig. 1.

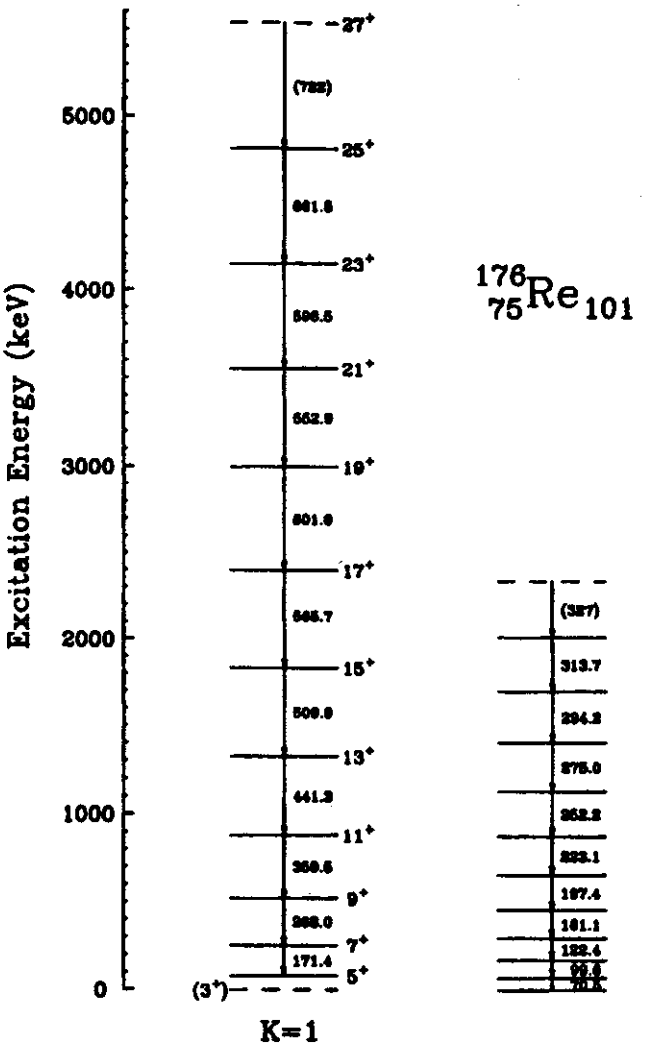

FIG. 2a: Partial level scheme of ^{176}Re.

Transitions within the $\Delta I=2$ doubly-decoupled bands were the most intense transitions in the spectra from all the reactions studied, and we were able to identify members of the bands up through $I^\pi=27^+$ in both ^{176}Re and ^{174}Re. Only odd-spin (negative-signature) states were populated,

the even-spin members presumably having been shifted to higher energies, making their population less favorable. The levels in these bands are shown in Figs. 2a and 2b.

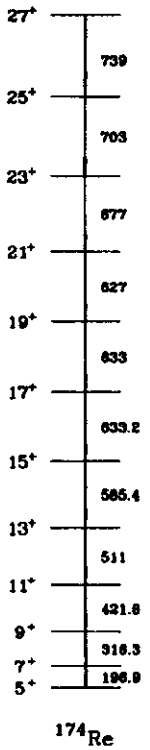

FIG. 2b: Partial level scheme of ^{174}Re.

It may seem surprising that $K=1$ bands are populated so strongly in heavy-ion reactions, which impart large amounts of angular momentum to the compound-nuclear system. However, this supports a mechanism akin to backbending[3]: The most efficient way of handling the larger amounts of angular momentum is a cooperation between the core and decoupled (rotationally- aligned) nucleons. Such decoupled states arise naturally from large-Ω orbits having large coriolis matrix elements, and once such "klokast" state are populated, the γ-ray depopulation tends to favor like states. Thus, only a select subset of the multitudinous odd-odd states is populated, and doubly-decoupled bands are the epitome of such klokast states.

A question arises concerning the lowest states in these bands. In ^{177}Re (nothing is known about ^{175}Re) the lowest state in the $1/2[541\downarrow]$ band is the $I=5/2$ member, forming a 3^+ lowest state for the doubly-decoupled band(s). IBFFA calculations (see below) also favor such a state. However, neither we nor Santos *et al.*,[4] who recently studied ^{176}Re, saw a $5^+ \rightarrow 3^+$ transition. Our calculations indicate it to be of the order of 80 keV or less, which could easily have been missed by both investigations.[5]

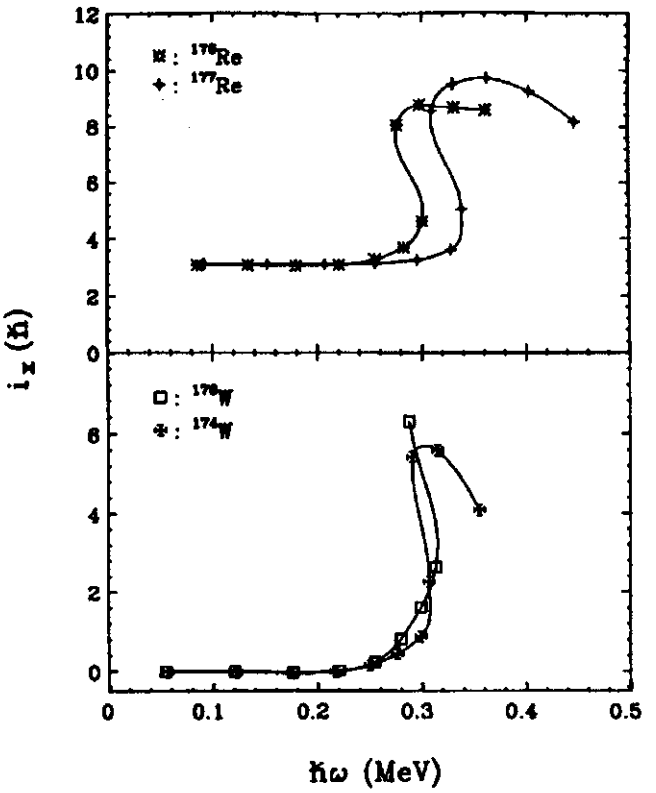

FIG. 3: Plot of alignment (i_x) versus rotational frequency ($\hbar\omega$) of ^{176}Re, ^{177}Re, ^{174}W, and ^{176}W.

The spacings of both doubly-decoupled bands are fairly regular at first, then they exhibit backbending. We thus plot the alignment, i_x, vs rotational frequency, $\hbar\omega$, for ^{176}Re, and compare it with ^{177}Re and nearby even-even W isotopes in Fig. 3. The crossing frequency in the ^{176}Re band is very close to that in ^{174}W and might even be slightly lower. Breaking of $i_{13/2}$ neutron pairs is typical of backbending for this mass region. The doubly-decoupled band does not occupy $i_{13/2}$ neutron states, so it does not block the available orbits for backbending. The odd neutron weakens the pairing, making backbending a little easier than in the even-even core nucleus. Conversely, its odd proton drives the nucleus toward larger deformation, making backbending more difficult. These two factors seem to cancel, resulting in nearly the same crossing frequency as in ^{174}W

(and ^{176}W). As a contrast, the odd-proton band in ^{177}Re backbends at a higher frequency because it does not have the odd neutron to compensate for the deformation change driven by the proton state.

We also performed extensive interacting-boson-fermion-fermion approximation (IBFFA, IBA extended to odd-odd nuclei) calculations for ^{180,182,184}Re, and these calculations reproduce the experimental results amazingly well.[6] These calculations reproduced a $\pi 1/2^-[541\downarrow]\times\nu 1/2^-$ band in all three nuclei, but the bands even predicted to lie rather high in energy in ^{182,184}Re. However, our calculations correctly predicted the band, with all of its severe coriolis distortions, in ^{180}Re.[7] Buoyed by this success, we extended our calculations to ^{176,178}Re, and our results for ^{176}Re are compared with experimental findings in Fig. 4.

The IBFFA calculations reproduce the features of the doubly-decoupled band very well, showing its even-spin numbers (and the 1^+ member) shifted to higher energies. The $K^\pi=0^+$ singlet couplings are also shifted up. We should emphasize that no experimental data yet exist for ^{175}Re, whose proton state couples with ^{177}Os to form ^{176}Re. Thus, we chose our IBFFA parameters (for ^{175}Re) from systematics. This makes the agreement even more surprising, since until now it has not been thought possible to use mere systematics when dealing with odd-odd calculations, especially when dealing with highly-distorted configurations such as these doubly-decoupled bands.

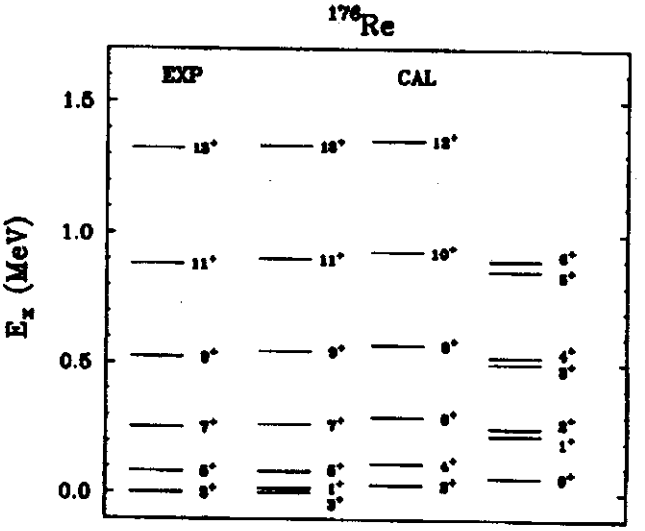

FIG. 4: Comparison of the IBFFA calculations for the doubly-decoupled band in ^{176}Re with experimental results.

References

1. A.J. Kreiner, D.E. DiGregorio, A.J. Fendrik, J. Davidson, and M. Davidson, Phys. Rev. C 29, 1572 (1984); Nucl. Phys. A432, 451 (1985).

2. Complete references given in W.A. Olivier *et al.*, MSUCL-702, (1989), submitted to Phys. Rev. C.

3. M.F. Slaughter, R.A. Warner, T.L. Khoo, W.H. Kelly, and Wm.C. McHarris, Phys. Rev. C 10, 656 (1984).

4. D. Santos *et al.*, Phys. Rev. C. 39, 902 (1989).

5. Wen-Tsae Chou, Ph.D. Thesis, Michigan State University (1989).

6. W.-T. Chou, Wm. C. McHarris, and O. Scholten, Phys. Rev. C 37, 2834 (1988).

7. W.-T. Chou, W.A. Olivier, R. Aryaeinejad, Wm.C. McHarris and O. Scholten, *Proceedings of the Conference on High-Spin Nucleus Structure and Novel Nucleus Shapes*, Argonne National Laboratory, 13-14 April 1988, p. 180 (1988).